Influence of electrolytes in the QCM response: Discrimination and quantification of the interference to correct microgravimetric data

João M. Encarnação [a], Peter Stallinga [b], Guilherme N.M. Ferreira [a],*

[a] *Centre for Molecular and Structural Biomedicine, University of Algarve, 8000 Faro, Portugal*
[b] *Centre of Electronics, Optoelectronics and Telecommunications, University of Algarve, 8000 Faro, Portugal*

Abstract

In this work we demonstrate that the presence of electrolytes in solution generates desorption-like transients when the resonance frequency is measured. Using impedance spectroscopy analysis and Butterworth–Van Dyke (BVD) equivalent electrical circuit modeling we demonstrate that non-Kanazawa responses are obtained in the presence of electrolytes mainly due to the formation of a diffuse electric double layer (DDL) at the sensor surface, which also causes a capacitor like signal. We extend the BVD equivalent circuit by including additional parallel capacitances in order to account for such capacitor like signal. Interfering signals from electrolytes and DDL perturbations were this way discriminated. We further quantified as $8.0 \pm 0.5 \, \text{Hz pF}^{-1}$ the influence of electrolytes to the sensor resonance frequency and we used this factor to correct the data obtained by frequency counting measurements. The applicability of this approach is demonstrated by the detection of oligonucleotide sequences. After applying the corrective factor to the frequency counting data, the mass contribution to the sensor signal yields identical values when estimated by impedance analysis and frequency counting.
© 2006 Elsevier B.V. All rights reserved.

Keywords: Quartz crystal microbalance; Piezoelectric sensor; Impedance analysis; Equivalent electrical circuit; Butterworth–Van Dyke model; Biosensor

1. Introduction

The integration of electronics and biology to produce biosensors has emerged in very recent years as an area of enormous potential (Willner and Wilner, 2001). The field of (bio)molecular sensors is now beginning to materialize as an aid to understand the underlying biophysical principles of molecular recognition as well as to detect the presence of specific analytes. Generally speaking, to reliably detect an event, and eventually to quantify the kinetics and affinity of molecule interaction, transduction into a measurable sensitive as well as selective signal is needed. Traditionally, transduction is achieved indirectly by gathering a signal generated by specific reporter groups, usually fluorescent or electrochemically active molecules, used to label the targeted analytes. These approaches require labelling the samples with the reporter groups prior to the sensing reaction. Sample labelling constitutes a possible source of error, irreproducibility, and contamination and is detrimental to the

sensitivity of the overall (bio)recognition analysis. The development of rapid, simple, selective and label-free methodologies for the detection of (bio)molecular recognition have thus been a long-standing goal. Piezoelectric transduction enables label-free detection of biorecognition events and has been used in microgravimetric devices, generally known as quartz crystal microbalance (QCM), for different applications (Pan et al., 1996; Yang et al., 1998; Etchenique and Brudny, 2000; Liu et al., 2004; Fabreguette et al., 2005; Su and Li, 2005; Wu et al., 2005; Modin et al., 2006).

The operation of a QCM relies on the piezoelectric effect, in which a quartz crystal is driven to mechanically resonate by application of a periodic electric field across its plane. The quartz crystal is the frequency determining element of an electric oscillator and the resonance frequency (f) and/or the frequency change (Δf) are measured. The data is often interpreted based on the Sauerbrey equation (Eq. (1)) which states that the measured frequency change (Δf) is linearly proportional to the mass load at the crystal exposed surface:

$$\Delta f_{\text{m}} = -\frac{2nf_0^2}{\sqrt{\rho_{\text{q}}\mu_{\text{q}}}}\frac{\Delta m}{A} = -C_{\text{f}}\frac{\Delta m}{A} \tag{1}$$

* Corresponding author. Tel.: +351 289800985; fax: +351 289818419.
E-mail address: gferrei@ualg.pt (G.N.M. Ferreira).

where f_0 is the resonant frequency of the fundamental mode, Δf_m the frequency change due to mass loading, n the harmonic number ($n = 1$ for the fundamental mode), ρ_q and μ_q, respectively, the density and the shear mode of the quartz material, Δm the mass change at the crystal surface, and A is the crystal sensitive area. The sensitivity factor (C_f) is a constant that only depends on physical parameters of the crystal sensor.

The Sauerbrey equation (Eq. (1)) makes the assumption that the mass deposited or the film formed at the surface of the crystal follows the vibration of the crystal and therefore the loaded crystal simply behaves as if it was thicker. Thus, this equation is only valid for thin, rigid, and uniform films. If the surface film is not entirely rigid, the quartz response depends not only on the mass load but also on the viscoelastic properties of the attached layer (Etchenique and Weisz, 1999; Lucklum and Hauptmann, 2000). Kanazawa and Gordon (1985) derived a relationship to account for the resonance frequency change of crystals in contact with liquids:

$$\Delta f_L = -f_0^{3/2}\sqrt{\frac{\rho_L \eta_L}{\pi \rho_q \mu_q}} \qquad (2)$$

where Δf_L is the frequency change due to liquid loading, ρ_L and η_L are the density and viscosity of the liquid in contact with the sensor surface, respectively. Therefore when detecting analytes in liquid environments both mass and liquid loading contribute to the total frequency change. Martin et al. (1991) have derived a model for the total frequency change accounting for the simultaneous contribution of mass and liquid loading to the sensor signal:

$$\Delta f = \Delta f_m + \Delta f_L = -\frac{2f_0^2}{n(C_{66}\rho_q)^{1/2}}\left[\frac{\Delta m}{A} + \left(\frac{\rho_L \eta_L}{4\pi f_0}\right)^{1/2}\right] \qquad (3)$$

where $C_{66} = 2.957 \times 10^{10}\,\text{nm}^{-2}$ is the stiffness of quartz (Martin et al., 1991).

Due to the additive nature of the mass and liquid loading (Eq. (3)) the mass effect cannot be differentiated when the frequency change is tracked, and, therefore, one has to be extremely careful when evaluating and interpreting the measured data. In spite of this apparent disadvantage, QCM sensors are still employed in a variety of applications using standard oscillator techniques and frequency counting, mainly due to its low cost and to the simplicity of the operation.

Impedance spectroscopy methods can provide more detailed information about the surface changes on QCM (Martin et al., 1991; Auge et al., 1995; Bouche-Pillon et al., 1995; Etchenique and Weisz, 1999; Lucklum and Hauptmann, 2000; Zhou et al., 2000a,b). A QCM sensor can be represented by a Butterworth–Van Dyke (BVD) model which consists of an equivalent electrical circuit representation of the system (Fig. 1) that is composed of a static capacitance (C_0) in parallel with a motional branch containing a inductance (L_m), a capacitance (C_m), and a resistance (R_m) in series—Area I in Fig. 1. The parameters of the equivalent electrical circuit are related to the ratio of energy stored in the oscillation and energy dissipation to the mounting structure of the crystal and contacting
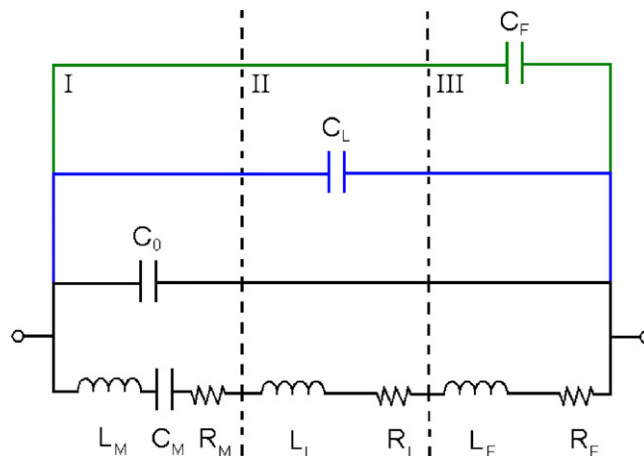
Fig. 1. Butterworth–Van Dyke equivalent circuit model (black circuit) and modified Butterworth–Van Dyke equivalent circuits to account for charged variation upon liquid (blue) and mass (green) loading. Area I, unloaded resonator; Area II, elements added due to liquid exposure; Area III, elements added due to the adsorption of mass on the surface of the sensor. (For interpretation of the references to colour in this figure legend, the reader is referred to the web version of the article.)

medium, i.e. viscous solutions and viscoelastic films (R_m); inertia to oscillation related to mass dislocation (L_m); oscillation energy storage related to the elasticity of the crystal (C_m); parasitic capacitance due to electrodes, holding structure, cables, and connectors (C_0). An advanced measurement system using a network or impedance analyzer enables the quantification of the different contributions R_m, L_m, C_m and C_0, by fitting the impedance/admitance spectrum around the crystal resonance frequency ($f = (4\pi^2 \times L_m C_m)^{-1/2}$) to the BVD model. The contribution of the different stages of the (bio)molecular recognition analysis can be evaluated by adding components to the BVD circuit—Areas II and III in Fig. 1 for liquid and mass loading, respectively—and by calculating the respective parameters.

Even though the quantification of the BVD model parameters enables the discrimination of the different contributions to the sensor signal at the different analysis stages, thus, significantly improving the sensor sensitivity by enabling the elimination of parasitic signals, impedance analysis and equivalent circuit modeling fails in discriminating, and thus in eliminating, the interference of charged molecules (Etchenique and Buhse, 2000, 2002). The presence of charged molecules in solution is known to introduce significant errors in the analytical quantification of adsorbed entities using QCM, even when using advanced impedance analysis (Etchenique and Buhse, 2000). In this work, we demonstrate that the presence of small electrolytes, as well as poly-ion molecules (using oligonucleotides as model) in QCM measurements generate strong interfering signals that cannot be eliminated by standard BVD equivalent circuit modeling. We propose a modification of the BVD model to account for such interferences (Fig. 1) and an example is given in which the modified model is used to the study of DNA hybridization and to correct frequency data, thus enabling the accurate quantification of the adsorbed mass.

2. Experimental

2.1. Reagents

All chemicals and reagents were ultra-pure, pro-analysis, or equivalent grade. Milli-Q water was used. Sodium dihydrogen phosphate, disodium hydrogen phosphate, sodium, potassium, calcium and magnesium chloride, absolute ethanol, and hydrogen peroxide were purchased from Merck. 11-Hydroxy-1-undecanothiol was purchased from Dojindo Molecular Technologies and 10 nm gold nanoparticles were purchased from Sigma.

Oligonucleotides were designed on the basis of human CTLA4 gene, purchased from Thermo Corporation at http://www.interactiva.de and used HPLC pure as received. 5′-Thiol modified oligonucleotide HS-Pr1 (GCT GAA CCT GGC TAC CAG GAC CTG GCC) was used to functionalize the sensor surface in order to detect the target complementary oligonucleotides Tgt1 (GGC CAG GTC CTG GTA GCC AGG TTC AGC) and HS-Tgt1. Tg1 and HS-Tg1 are identical and fully complementary to HS-Pr1 except that HS-Tgt1 is thiol modified to enable labeling with gold nanoparticles (see below).

An oligonucleotide sequence with null complementarity with both the probe and target sequences was used as control—Ctr1 (TAG GAG GTC ATC TCG AGC TAT GGC TCT GTT ATT AGC).

2.2. Oligonucleotide labeling with gold nanoparticles

Oligonucleotides were labeled with gold nanoparticles following a previously published protocol (Csáki et al., 2003). Briefly, 35 µl of a 100 µm solution of HS-Tgt1 were diluted in 5 ml of a 8.7 nm colloidal aqueous solution of 10 nm gold nanoparticles and incubated at room temperature for 16 h. After diluting the reaction mixture with 5 ml of PBS buffer (100 mm phosphate containing 100 mm NaCl, pH 7.0) and incubating at room temperature for 30 h, 11-hydroxy-1-undecanothiol was added to a final concentration of 50 µM and the mixture was incubated at room temperature for additional 12 h. Modified nanoparticles were recovered by centrifugation for 30 min at 12 000 rpm, washed twice with 5 ml PBS, and dispersed in a PBS buffer.

Control gold nanoparticles (Au-SAM nanoparticles) were prepared similarly using Milli-Q water instead of the HS-Tgt1 solution.

2.3. Quartz crystal sensors

One inch diameter 5 MHz AT-cut quartz crystals, coated with optically flat polished gold electrodes on both sides, were purchased from Stanford Research Systems (SRS, Stanford, USA). The active area and sensitivity factor of the crystal are $A = 0.4\,cm^2$ and $C_f = 56.6\,Hz\,cm^2\,\mu g^{-1}$, respectively.

The crystals were cleaned before use by rinsing with absolute ethanol and Milli-Q water before immersion in Piranha solution (30%(v/v), H_2O_2:H_2SO_4 = 1:3) for 15 min, to obtain a clean gold surface. Cleaned crystals were then rinsed with water and dried in a nitrogen stream.

2.3.1. Quartz crystal sensor functionalization

To functionalize the surface of the crystal sensors, 50 µl of a 5 µm solution of probe HS-Pr1, freshly prepared in PBS buffer, were carefully pipetted onto the surface of a cleaned crystal sensor, and incubated at room temperature for 5 h in a humidified chamber. Unbounded probe was removed by washing the functionalized crystal sensors sequentially with PBS buffer and Milli-Q water. After drying under a nitrogen flow, the functionalized crystal sensors were incubated overnight, at room temperature in an humidified chamber, with 100 µl of a 50 µm 11-hydroxy-1-undecanothiol 10% (v/v) ethanolic solution in order to completely cover exposed surface areas, to remove unspecificaly adsorbed HS-Pr1 probe, and to better organize the monolayer (Herne and Tarlov, 1997).

Control sensors were prepared similarly with the sole difference that clean crystals were incubated with 50 µl PBS buffer instead of HS-Pr1 probe.

2.4. Experimental set-up

Cleaned or functionalized sensors were mounted on a Kynar crystal holder (SRS) with a home-made acrylic cover to form a 300 µl flow cell exposing just one face of the sensor to the solution. Viton O-rings were placed underneath the sensor, sealing the flow cell to avoid wetting or flooding the electrical contacts located on the bottom of the crystal holder. A closed-cycle fluidic circuit was mounted using Tygon tubing to connect the flow cell to an agitated container where all the samples are added. The total volume of the systems is 2 ml and the solutions were recirculated in the system at a flow rate of 500 µl min^{-1} controlled by a Watson–Marlow peristaltic pump. Both the flow cell and the container were installed in a home-made 1l jacketed beaker to control the temperature of the system at $25 \pm 0.1\,°C$ by means of a Thermo Haake temperature controller.

The resonance frequency and impedance spectra were recorded alternatingly using a QCM100 Controller and a QCM25 Oscillator (SRS) connected to a Pendulum CNT-66 frequency counter or using a RF HP8712C Network Analyzer, respectively. The network analyzer and the QCM25 Oscillator were electrically connected to the crystal holder through an electronic switch used to select the desired measurement mode. The instruments were interfaced to a computer through IEEE boards and custom made acquisition programs.

2.5. Impedance analysis

Impedance spectra were obtained using a 10 kHz frequency span centred near the crystal's resonant frequency with 16 spectra averaging at 1 Hz resolution.

The BVD equivalent circuit parameters were obtained from the experimental data by calculating the conductance function $(|Y| = |Z|^{-1}$; $|Z|$ being the recorded impedance magnitude) and fitting, using a fitting routine written in Matlab, to the following

equations:

$$|Y| = \sqrt{\left(\frac{R_m}{R_m^2 + U^2}\right)^2 + \left(\omega C_0 - \frac{U}{R_m^2 + U^2}\right)^2} \quad (4)$$

$$U = \omega L_m - \frac{1}{\omega C_m} \quad (5)$$

where $\omega = 2\pi f$ is the angular frequency.

The analysis is initialized by estimating the four BVD parameters (R_m, L_m, C_m and C_0) for the crystal sensor exposed to air. Typical parameters for air exposed crystal sensors in the experimental set-up used are $R_m = 12.925\ \Omega$, $L_m = 33.725$ mH, $C_m = 29.925$ fF, and $C_0 = 184.575$ pF, respectively. Since C_m is related only to the sensor physical material, it is constant within the experiments. The successive contributions of solvents and adsorbed mass are thus obtained by a three parameter fitting (R_m, L_m, C_0) of the respective conductance functions. This procedure is repeated for each stage of the experiment and the BVD parameters of the particular experimental stage, thus of the individual contributions, are calculated by subtracting the global parameters, obtained by fitting, from the respective parameter calculated for the previous stage of the experiment. To facilitate data analysis it is usual to represent a parameter XL which is the sensor inductance in resistive units (Ω) obtained by multiplying the calculated inductance value by the angular frequency $\omega = 2\pi f$.

3. Results and discussion

3.1. Effect of small increments of electrolytes

Considering the use of QCM devices in (bio)molecular sensing and recognition, where in the majority of the situations the analytes are present in buffered solutions containing small amounts of electrolytes, a set of experiments was undertaken to study and characterize the influence of such electrolytes in the sensor signal. Milli-Q water was circulated in the sensor flow chamber and, after establishing a stable resonance frequency signal, small volume amounts of concentrated solutions of NaCl, KCl, MgCl$_2$ or CaCl$_2$ were successively added in the sample container in order to achieve the desired ionic strength in the system. As shown in Fig. 2, the QCM sensor responds strongly to small variations on the solution electrolyte concentration when the resonance frequency is directly measured by frequency counting. To evaluate if this response is related to eventual variations of the hydrostatic pressure, owing to the small volume increments, control experiments were performed where similar volume amounts of Milli-Q water were added instead of electrolyte solutions. No frequency variations were observed for these control experiments which indicate that the frequency variations observed (Fig. 2) are related to nothing more than the presence of the electrolytes. Fig. 2 also shows that monovalent and divalent cations affect the frequency variation (Δf) differently. Even though the general tendency is the same, with frequency decreasing for the initial variations and increasing after reaching a minimum, the frequency increase rate is
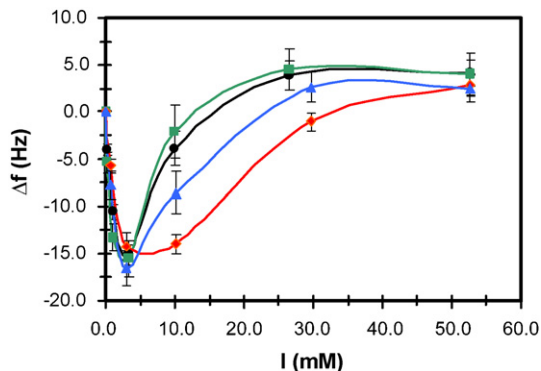
Fig. 2. Average ($n = 6$) resonance frequency variation (Δf) with increasing ionic strength for (●) NaCl, (■) KCl, (♦) CaCl$_2$ and (▲) MgCl$_2$.

higher for monovalent cations (Na$^+$ and K$^+$) when compared to divalent cations (Mg^{2+} and Ca^{2+}).

If one adopts the mathematical models usually used to interpret frequency variation data (Eqs. (1)–(3)), the increase in the frequency observed (Fig. 2) should be related either to a decrease of the mass over the crystal surface or to a decrease in the solution viscosity and/or density. Considering that: (i) the bulk solution viscosity and density are unchanged during the experiments; (ii) no mass is deposited over the crystal; (iii) the addition of such small quantities of salt has negligible or no effect on the overall system hydrostatic pressure, we propose, in accordance with previously published work (Etchenique and Buhse, 2000), that the anomalous frequency response observed is correlated to the increment of the charge density in the solution due to the addition of electrolytes.

The admittance data associated with the experiments described above were recorded, in order to investigate in more detail the origins of the frequency variation, to differentiate the effect of the different interferences, and to calculate the values of the parameters of the BVD equivalent electrical circuit. Fig. 3 shows the variation of each parameter with the small increments of the solution ionic strength. In accordance with previously published data (Etchenique and Buhse, 2000; Ghafouri and Thompson, 2001), the calculated inductance and resistance increase with increasing ionic strength. This increase occurs up to reaching a certain ionic strength, after which the inductance stabilizes while resistance decreases considerably (Fig. 3A and B). On the basis of the BVD parameters it is possible to predict the resonance frequency variation ($f = (4\pi^2 \times L_m C_m)^{-1/2}$). Fig. 3C shows that the predicted frequency variation with the solution ionic strength is not consistent with the measured values. Even though sharing a similar tendency for the low ionic strengths, with resonance frequency decreasing with increasing ionic strengths, for the higher ionic strengths the predicted resonance frequency variation stabilizes close to its minimum value while the measured resonance frequency variation considerably increases before stabilizing. Furthermore, contrary to the measured data, impedance analysis predicts different sensor responses to mono and divalent cations (Fig. 3C). These results suggest that QCM frequency counting data is affected by interfering signals which can be avoided or eliminated by using full impedance analysis.
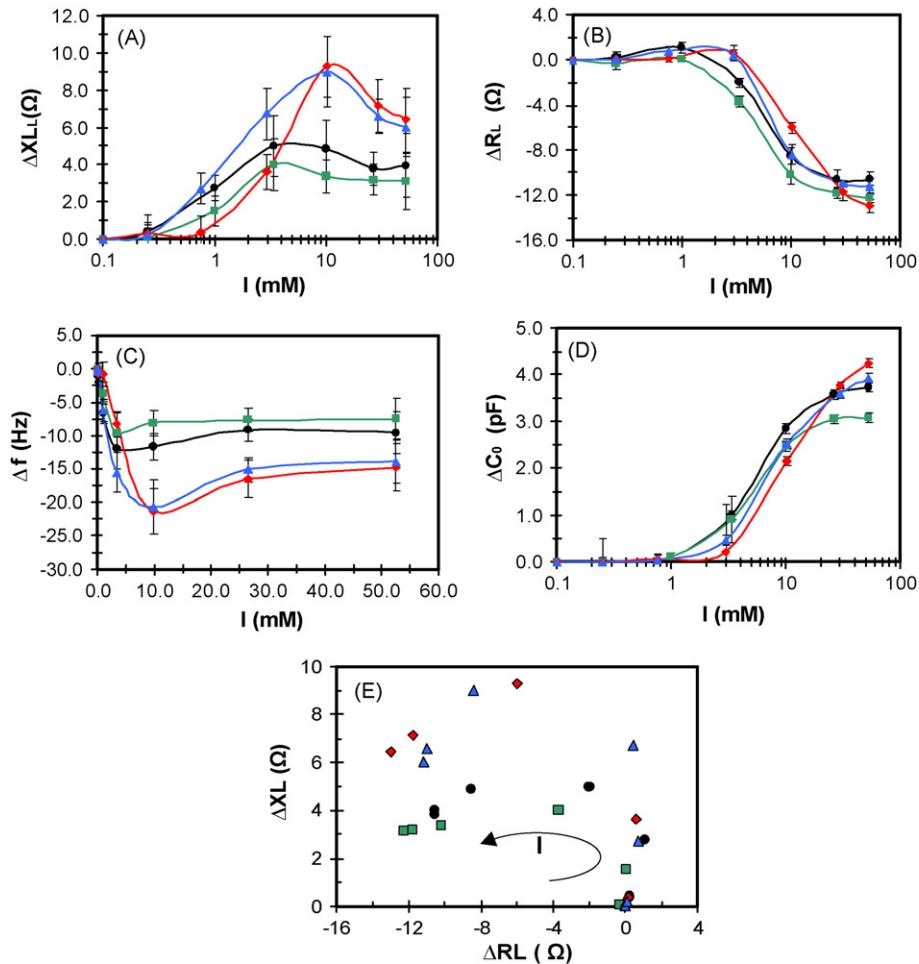
Fig. 3. Variation of the Butterworth–Van Dyke model parameters with the ionic strength for (●) NaCl, (■) KCl, (♦) CaCl$_2$ and (▲) MgCl$_2$: (A) inductance; (B) resistance; (C) calculated resonance frequency variation; (D) parallel capacitance; (E) parametric polar impedance plot. The figures correspond to the average of impedance analysis data resulting from three independent experiments for each data point.

Owing to the assumption that the parallel capacitance (C_0) is related to the physical properties of the system components, such as electrodes, cables, connectors, and holders, this capacitance was expected to be constant within the experiments. Contrary to these expectations, C_0 also increases with increasing the ionic strength (Fig. 3D). This result suggests that variations in the electrolyte composition of the solution results in a capacitive response characterized by a specific addition to C_0. To account for such sensor response, in accordance with previously published experimental work (Xie et al., 2001), we extended the generally used BVD model to include additional capacitances in parallel for each stage of the experiment (Fig. 1). We expect that these additional capacitances will enable the differentiation of the influence of charged species added or removed in each stage, thus the correction of calculated parameters upon rendering the parasitic capacitance (C_0) constant. According to this modification, the parallel capacitance calculated corresponds to the total parallel capacitance of the system ($C_T = C_0 + C_L + C_F$) and includes the contributions from the static capacitance (C_0), and the additional capacitances due to charge variation upon liquid loading (C_L) and/or mass loading (C_F). The influence of the charge variation at a given stage is this way discriminated after

subtracting the capacitance values calculated for the previous stages.

Further interpretation of the calculated parameters reveals no variation of the resistance (R) or the capacitance (C_0) with the cation valence (Fig. 3B and D). On the other hand, the simultaneous determined inductance values (Fig. 3A) reveal a strong influence by the cation valence, a result that is consistent with the data gathered by frequency counting (Fig. 2). As shown in Fig. 3A, the resonator inductance increases to a further extent, both considering the amplitude and the ionic strength, when divalent cations are present. Since the resonance frequency is affected by the motional inductance and capacitance ($f = (4\pi^2 \times L_m C_m)^{-1/2}$) these results show that, for the same ionic strength, divalent cations generate higher frequency drops and slower responses to ionic strength variations which are driven just by the inductive contribution of the resonator.

3.2. Piezoelectric resonators sense and respond to modifications of the diffusive electrical double layer

Considering the physical meaning of the BVD parameters, in particular the fact that XL is related to vibrating mass, hence

reflecting mass displacement, and that R is related to acoustic energy loss owing to medium damping (viscous losses), a more detailed analysis of the experimental data reveals that the recorded profiles, both by frequency counting and impedance measurements, can be divided into two distinct regions. In the low ionic strength region ($I < 1$ mM) the resonant frequency drops while both the calculated inductance and resistance rise. This is compatible to an increase of the density and/or of the viscosity near the crystal's surface. On the other hand, for higher ionic strengths ($I > 1$ mM) the resonant frequency increases and the resonator impedance is characterized by $XL \gg R$ which indicates the formation of a rigid enough layer that moves in phase with the resonant surface.

It seems thus that a layer is formed at the crystal surface whose viscosity/rigidity depends on the solution electrolyte nature and composition. The viscoelastic behavior of this layer can be characterized by the parametric polar impedance plots, which are graphical representations of the variation of the calculated inductance with the variation of the calculated resistance (Fig. 3E). In general, parametric polar impedance plots of Newtonian or viscoelastic fluids are characterized by linear relationship between of XL and R whose slope equals 1 for Newtonian fluids (Etchenique and Buhse, 2002). On the other hand, fluids or layers of variable viscosity or elasticity are characterized by a curvature in the XL versus R plots (Etchenique and Buhse, 2002). As such, the circular shape of the XL versus R plots of Fig. 3E leads to the conclusion that a thin film with variable viscosity/elasticity is formed between the crystal surface and the solution bulk.

Considering that the solutions in contact with the crystal surface consist of water and electrolytes, the only possible layer being formed or "deposited" on the crystal surface is a diffuse electrical double layer (DDL). The thickness of the DDL, the Debye length, is known to be influenced by the concentration and by the valence of electrolytes (Atkins, 1990). By increasing the solution ionic strength, or by using ions with higher valences, the Debye length decreases, resulting in a reduced distance between charged particles, as well as the entire double layer drawing nearer the surface, resulting therefore in the accumulation of charges at the electrode's surface. Thus, more rigid films and higher charge accumulation are expected to be

formed close to the sensor surface for higher ionic strengths and valences, detected by higher inductance values (Fig. 3A). Moreover, higher capacitances (Fig. 3D) are measured as a consequence of the additional parallel capacitances.

3.3. Use of modified BVD data as corrective tool to evaluate and quantify DNA hybridization

To further demonstrate the applicability of the proposed modification to the BVD model we evaluated the sensor response as a DNA detector. DNA fragments, and oligonucleotides, are polyelectrolytes in neutral aqueous solution and a strong interfering signal resulting from DDL perturbation can be expected. Crystal sensors were functionalized with oligonucleotides, mounted in the experimental set-up, and used to detect complementary oligonucleotides (Fig. 4). As shown in Fig. 4A, the signals measured by frequency counting for unlabeled oligonucleotides and for the controls are similar. Such a result leads to the conclusion that either the sensor is not fully operational or no complementary sequences are present. The lack of signal variation in frequency counting measurements when using unlabeled oligonucleotide or DNA fragments has been reported by other authors that used gold nanoparticles as labels for mass amplification in order to force a signal resulting from DNA hybridization at the sensor surface (Zhou et al., 2000a,b; Su and Li, 2005). Even though resonance frequency variations are measured when using gold labeled targets (Fig. 4A), target labeling withdraws from piezoelectric sensors the advantages of direct transduction of unlabeled targets. Moreover, the total frequency variation obtained for the gold labeled oligonucleotides measured by frequency counting is $\Delta f = 19$ Hz (Fig. 4A) which only accounts for 63% of the frequency change predicted from impedance analysis data (Fig. 4B). This discrepancy indicates that quantitative calculations based on frequency counting (e.g. mass determination) can be underestimated due to the interfering signal resulting from the effect of the charges on the sensor surface and adjacent layers.

In order to account for the effects of charges we propose the calculation of the respective interfering capacitances C_L and C_F (Fig. 1). The total frequency variation (Δf_T) due to mass
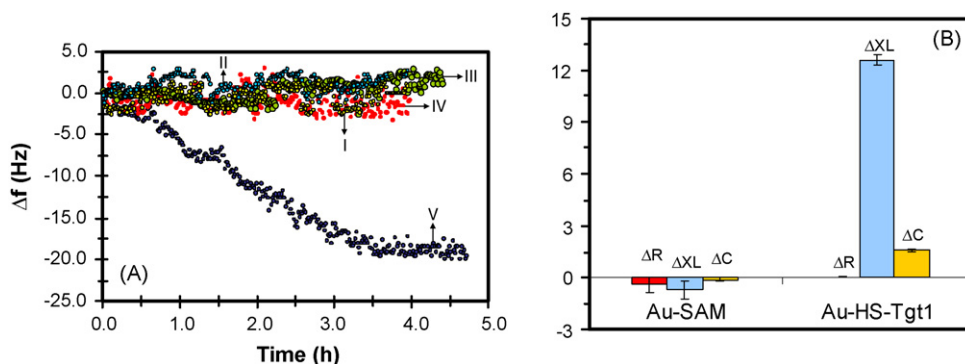
Fig. 4. Crystal sensor response to DNA hybridization. All crystal sensors used were functionalized with HS-Pr1 probe and blocked with 11-hydroxy-1-undecanothiol: (A) resonance frequency recorded for crystal sensors incubated with (I) PBS buffer, (II) 1 µM of Ctr1, (III) 1 µM of Tgt1, (IV) 1.7 nM of Au-SAM nanoparticles, (V) 1.7 nM of Au–HS-Tgt1 nanoparticles; (B) impedance data acquired for crystal sensors incubated with gold nanoparticles modified with 11-hydroxy-1-undecanothiol (Au-SAM) and gold nanoparticles functionalized with complementary target HS-Tgt1 (Au–HS-Tgt1).

loading (Δf_M), viscoelasticity of the adsorbed/deposited mass (Δf_V), liquid (Δf_L) and charge interference (Δf_C) should be thus obtained by:

$$\Delta f_T = \Delta f_M + \Delta f_V + \Delta f_L + \Delta f_C \qquad (6)$$

When operating the QCM in the oscillator/frequency counting mode in liquid phase (Δf_M), (Δf_V), (Δf_C) can not be differentiated, and the measured frequency variations is given by $\Delta f_T - \Delta f_L$. In analogy to the case of the generally accepted correction for the liquid loading effects, where the contribution of the buffer viscosity/elasticity and density to the total frequency change (Δf_L) is estimated from a linear relationship established between Δf and ΔR (Martin et al., 1991; Zhou et al., 2000a,b), we seek for a parameter that could be used to correct the underestimation of frequency counting quantification. Considering, once again, that the frequency variations shown in Figs. 2 and 3, results only from charge interferences ($\Delta f_M = \Delta f_L = \Delta f_V = 0$), we used the data from these figures to estimate the values of such a parameter. A plot of the measured frequency variation against the calculated interfering capacitance (Fig. 5) shows that these parameters are linearly correlated within the range investigated, leading to the conclusion that the frequency variation is linearly dependent on the calculated capacitance variation (demonstrated by the close to one correlation coefficients and by the *p*-values (Fig. 5). Moreover, the similarity of the slopes may indicate that the observed frequency variations are due to the capacitive effect and could be independent on the charged species involved. Thus, calculating the average of the slopes we find a frequency variation of 8.0 ± 0.5 Hz pF^{-1} resulting from charge interference. To test the applicability of this hypothesis we apply this corrective factor to the data gathered for the gold labeled oligonucleotide detection (Fig. 4). For this case, the charge interference was quantified as $C_F = 1.60 \pm 0.02$ pF (Fig. 4B) which results in an estimated contribution to the frequency variation of $\Delta f_C = 12.8 \pm 0.8$ Hz. Since the immobi-

lized mass has a negligible viscous effect ($\Delta R \approx 0$, Fig. 4B), the use of Eq. (6) estimates the frequency variation due to mass load as $\Delta f_M = \Delta f_T - \Delta f_L + \Delta f_C = 31.8$ Hz. The similarity between this value and the 30 Hz estimated from the impedance data demonstrates that charge interferences can reliably be corrected by using the parameter obtained from Δf versus ΔC correlations.

4. Conclusions

In this work, we demonstrated that the response of QCM is affected by the presence of electrolytes in solution. This interference leads to transients mimicking desorption, with frequency variations (Δf) decreasing with increasing densities of charges in solution, and can thus have a considerable impact in biosensor applications, up to the point of leading to less accurate conclusions. The influence of electrolytes results in non-Kanasawa response, which, for the low ionic strengths, is characterized by a frequency drop and by an increase of the sensor inductance and resistance owing to the increase of the density and viscosity near the sensor surface as a diffuse electric double layer develops. For high ionic strengths, charge effects predominate, leading to increasing resonance frequencies, while the resistance drops and the parallel capacitance increases. We propose a modification to the Butterworth–Van Dyke model to include additional parallel capacitances in order to account for the influence of charges to the sensors response. Such influence is linearly correlated with the measured resonance frequency variation in the range of 1 mM $\leq I \leq 50$ mM and is characterized by a desorption-like signal of 8.0 ± 0.5 Hz pF^{-1}. The use of this factor allows for the correction of the mass-frequency variation, which otherwise is close to 40% underestimated, resulting in a convergence of the values measured by frequency counting and impedance analysis. Estimating the influence of electrolytes and its contribution to the measured frequency variation thus enables the acquisition of more accurate data and this represents a step forward in the use of piezoelectric sensors for quantitative direct transduction of molecular recognition events.

Fig. 5. Relationship between measured resonance frequency variation and calculated parallel capacitance in the range of 1 mM $\leq I \leq 50$ mM. Triplicate independent experiments for (●) NaCl (12 experimental points), (■) KCl (12 experimental points), (◆) CaCl$_2$ (12 experimental points), and (▲) MgCl$_2$ (9 experimental points) were performed; linear regression of experimental data yielded the correlations $\Delta f = (7.8 \pm 0.4) \times \Delta C + (-24 \pm 1)$, $r = 0.9862$, $p < 0.0001$, for NaCl, $\Delta f = (8.7 \pm 0.3) \times \Delta C + (-23.6 \pm 0.8)$, $r = 0.9935$, $p < 0.0001$, for KCl; $\Delta f = (7.8 \pm 0.5) \times \Delta C + (-31 \pm 2)$, $r = 0.9790$; $p < 0.0001$, for CaCl$_2$; $\Delta f = (7.7 \pm 0.9) \times \Delta C + (-28 \pm 4)$, $r = 0.9372$, $p = 0.0002$ for MgCl$_2$.

References

Auge, J., Hauptmann, P., Hartmann, J., Rösler, S., Lucklum, R., 1995. Sens. Actuators B 24, 43–48.

Atkins, P.W., 1990. Physical Chemistry, 4th ed. Oxford University Press, UK.

Bouche-Pillon, D., Gabrielli, C., Perrot, H., 1995. Sens. Actuators B 25, 257–259.

Csáki, A., Kaplanek, P., Möller, R., Fritzche, W., 2003. Nanotechnology 14, 1262–1268.

Etchenique, R., Weisz, A.D., 1999. J. Appl. Phys. 86 (4), 1994–2000.

Etchenique, R., Brudny, V.L., 2000. Langmuir 16, 5064–5071.

Etchenique, R., Buhse, T., 2000. Analyst 125, 785–787.

Etchenique, R., Buhse, T., 2002. Analyst 127, 1347–1352.

Fabreguette, F.H., Sechrist, Z.A., Elam, J.W., George, S.M., 2005. Thin Solid Films 488 (1/2), 103–110.

Ghafouri, S., Thompson, M., 2001. Analyst 126, 2159–2167.

Herne, T.M., Tarlov, M.J., 1997. J. Am. Chem. Soc. 119, 8916–8920.

Kanazawa, K.K., Gordon, J.G., 1985. Anal. Chim. Acta 175, 99–105.

Liu, Y., Zhang, W., Yu, X., Zhang, H., Zhao, R., Shangguan, D., Li, Y., Shen, B., Liu, G., 2004. Sens. Actuators B 99, 416–426.

Lucklum, R., Hauptmann, P., 2000. Sens. Actuators B 70, 30–36.

Martin, S.J., Granstaff, V.E., Frye, G.C., 1991. Anal. Chem. 63, 2272–2281.

Modin, C., Stranne, A.-L., Foss, M., Duch, M., Justesen, J., Chevallier, J., Andersen, L.K., Hemmersam, A.G., Pedersen, F.S., Besenbacher, F., 2006. Biomaterials 27, 1346–1354.

Pan, W., Durning, C.J., Turro, N.J., 1996. Langmuir 12, 4469–4473.

Su, X.-L., Li, Y., 2005. Biosens. Bioelectron. 21 (6), 840–848.

Willner, I., Wilner, B., 2001. Trends Biotechnol. 19, 222–230.

Wu, T.-Z., Su, C.-C., Chen, L.-K., Yang, H.-H., Tai, D.-F., Peng, K.-C., 2005. Biosens. Bioelectron. 21 (5), 689–695.

Xie, Q., Zhang, V., Xiang, C., Tang, J., Li, Y., Zhao, Q., Yao, S., 2001. Anal. Sci. 17, 613–620.

Yang, M., Yau, H.C.M., Chan, H.L., 1998. Langmuir 14, 6121–6129.

Zhou, X.C., O'Shea, S.J., Li, S.F.Y., 2000a. Chem. Commun. 11, 953–954.

Zhou, A., Zhang, J., Xie, Q., Yao, S., 2000b. Sens. Actuators B 67, 68–75.